A Single Organoiridium Complex Generating Highly Active Catalysts for both Water Oxidation and NAD+/NADH Transformations

(Article begins on next page)

07 February 2025

A Single Organoiridium Catalyst Exhibiting High Activity in both Water Oxidation and NAD+/NADH Transformations

Alberto Bucci,[a†*] Savannah Dunn,[b§] Gianfranco Bellachioma,[a] Gabriel Menendez Rodriguez,[a] Cristiano Zuccaccia,[a] Carlo Nervi,[c] and Alceo Macchioni[a,d*]

[a]Department of Chemistry, Biology and Biotechnology, University of Perugia and CIRCC, Via Elce di Sotto, 8, I-06123 Perugia, Italy. [b]Department of Chemistry, Longwood University 201 High Street, Farmville, VA, 23901, USA. [c]Department of Chemistry, University of Torino, Via Pietro Giuria 7, 10125 Torino, Italy. [d]Department of Chemistry and Applied Biosciences, ETH Zürich, Vladimir-Prelog-Weg 2, CH-8093, Switzerland.

ABSTRACT: The complex $[Cp^*Ir(pica)Cl]$ (**1**, pica = picolinamide = κ^2-pyridine-2-carboxamide) was found to be an effective catalyst for both water oxidation to molecular oxygen and NAD+/NADH transformations, which are the key reactions of light dependent natural photosynthesis. In particular, **1** exhibits high activity in water oxidation driven by CAN and $NaIO_4$. With the former, the initial TOF exceeds that of $[Cp^*Ir(pic)Cl]$ (**2**, pic = picolinate = κ^2-pyridine-2-carboxylate), which is the fastest iridium catalyst reported to date, whereas with $NaIO_4$ it compares well with the best catalysts. **1** exhibits top performances also in the hydrogenation of NAD+ with HCOOK leading to the regiospecific formation of 1,4-NADH (pH 7) with TOF = 143 h^{-1}, which is about three times higher than the previous highest value (54 h^{-1}) reported for $[Cp^*Ir(4-(1H-pyrazol-1-yl-\kappa N^2)benzoic\ acid)(H_2O)]SO_4$ (**3**). Activity seems to be critically affected by the presence of the NH-functionality, as indicated by its drop of about one order of magnitude when **2** (TOF = 17 h^{-1}) was used as the catalyst instead of **1**. **1** is also capable to mediate the dehydrogenation of β-NADH, under slightly acidic conditions, as determined by NMR and GC measurements. Furthermore, an in-depth investigation carried out combining 1D, 2D and diffusion NMR techniques indicate a remarkable speciation of β-NADH leading not only to the expected β-NAD+ but also to α-NAD+, nicotinamide (NA) and 1,2,5,6-tetrahydronicotinamide (NAH₃). The formation of NAH₃ has been identified as the cause of the low TON values obtained with **1** and **3**, because it consumes part of the produced H_2.

INTRODUCTION

The photosynthesis of solar fuels from abundant raw materials is considered one of the most promising strategies to sustain the increasing worldwide level of energy consumption of our society. [1,2,3,4] Inspiration for developing an efficient photosynthetic apparatus has traditionally derived from Nature,[5] who, over the course of many billions of years, according to the evolutionary theory, has set up a wonderful machinery capable of converting carbon dioxide and water in carbohydrates, using the energy of the sunlight to permit the otherwise endergonic process to occur.[6]

$$2H_2O + 2NADP^+ + 8h\nu \rightarrow 2NADPH + 2H^+ + O_2 \quad (1)$$
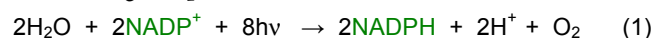
At the heart of such machinery, key roles are played by two catalytic pools (oxygen evolving complex, OEC;[7,8] ferredoxin/ferredoxin NADP+ reductase[9,10,11]), which offer viable kinetic pathways to both the oxidation of water and reduction of NADP+.[12] The reaction of water with NADP+ (eq. 1), which is the net electron transfer reaction of Z scheme of oxygenic photosynthetic organisms, leads to the formation of

NADPH, successively used to reduce CO_2 in light-independent reactions, and O_2.[6]

Many organometallic complexes have been successfully exploited to independently catalyze water oxidation (WO),[13,14,15,16,17,18,19,20,21,22] hydrogenation of NAD+,[23,24,25,26,27,28,29,30,31,32] and dehydrogenation of NADH.[33,34] Nevertheless, to the best of our knowledge, only the complexes $[Cp^*Ir(N,N)Cl]Cl$ (N,N = 2,2'-bipyridine, bpy, and 1,10-phenantroline, phen) were found to be competent catalysts for both WO[14] and NAD+ hydrogenation.[33]
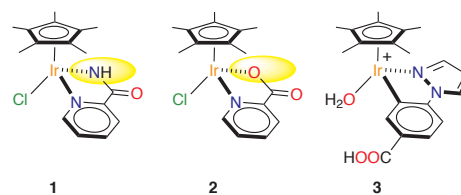

Chart 1. Catalysts considered in this study.

Herein we report on the catalytic performance of complex $[Cp^*Ir(pica)Cl]$ {pica = picolinamide = κ^2-pyridine-2-carboxamide, ion(−1), **1**}[35] (Chart 1) toward both WO,

driven by cerium ammonium nitrate (CAN) and NaIO$_4$, hydrogenation of NAD$^+$ with HCOOK and dehydrogenation of NADH. In all reactions **1** exhibits very high/top performances. The rationale behind the design, synthesis and catalytic applications of **1** is threefold. First, in our search for an efficient and robust catalyst for WO we found that [Cp*Ir(pic)X]^{22} {pic = picolinate = κ^2-pyridine-2-carboxylic acid, ion(−1), X$^−$ = Cl$^−$ (**2**, Chart 1) and NO$_3^−$} precursor and its derivatives having an OH-substituent in one of the pyridine ring positions are extremely active.[36] The picolinate is a strongly electron donating ligand that facilitates the oxidative steps of WO cycle, whereas OH-substituents finely modulate, in a pH-responsive fashion, the catalytic activity. We thought that the substitution of the carboxylate group in **1** with the isolelectronic amidate group (highlighted in yellow in Chart 1) might lead to a still active WO catalyst since a similar and even a little higher electron density should be donated to the metal center. Second, having an –NH functionality in close proximity to the metal could be beneficial for bringing about hydrogenation and dehydrogenation reactions of NAD$^+$ and NADH, respectively, through the establishing of substrate/catalyst hydrogen bonds.[37,38,39,40] Third, κ^2-pyridine-2-carboxamide ligand is clearly biomimetic and might induce a higher affinity of **1** with NAD$^+$ and NADH.

RESULTS AND DISCUSSSION

Complex **1**[41] was synthesized by the reaction of the iridium dimer precursor [Cp*IrCl$_2$]$_2$ and 2-picolinamide in methanol at room temperature, in the presence of 2 equivalents of potassium hydroxide (Scheme 1).
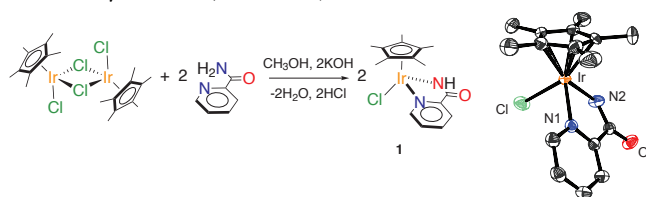
Scheme 1. Synthesis and an ORTEP view (ellipsoid are drawn at 50% probability level) of complex 1. Selected bond distances (Å) and angles (deg): Ir–N1 = 2.101(3), Ir–N2 = 2.082(4), Ir–Cl = 2.4125(15), Ir–Cp* = 1.775(4); N1–Ir–N2 = 76.18(15), N1–Ir–Cl = 85.09(10), N2–Ir–Cl = 91.07(13), Cp*–Ir–N1 = 133.07(17), Cp*–Ir–N2 = 129.59(7), Cp*–Ir–Cl = 125.67(43). Cp* is the centroid of the Cp* ring.

The characterization of **1** in solution was accomplished by combining all pieces of information coming from ^{1}H and ^{13}C 1D and 2D NMR experiments (Supporting Information, SI, Figure S1-S5). Crystals suitable to be analyzed by X-Ray diffractometry were obtained by slow diffusion of n-hexane into a solution of **1** in dichloromethane. An ORTEP representation of the structure in the solid state is reported in Scheme 1. Complete crystallographic data are given in SI.

Characterization data of **1** do not show any particular feature but confirm that the electron density at the metal center is slighter higher than that in **2**.[36] This is evidenced in the solid state by the Ir–Cl [2.4125(15) Å *versus* 2.3997(15) Å] and Ir–Cp* [1.775(4) Å *versus* 1.764(3) Å] distances that are longer than in **2**.[36] In solution, the quaternary carbon of Cp* falls at a higher chemical shift in **1** (86.3 ppm) than in **2** (84.9 ppm), whereas cyclic voltammetry (CV) experiments (SI, Figure S6) show an irreversible oxidation process, occurring at 0.95 V *versus* SCE, which is at considerably lower potential than for **2** (1.2 V).[36]

Water Oxidation. The catalytic activity of complex **1** toward WO was studied using CAN and NaIO$_4$ as sacrificial oxidants, measuring oxygen evolution kinetics by means of differential manometry and Clark electrode. In addition, Ce^{4+} depletion kinetics was followed by UV-Vis spectroscopy in the case of CAN driven WO. A summary of the catalytic results is reported in Table 1.

Table 1. Kinetic data for water oxidation catalyzed by 1 (25 °C, H$_2$O).

Entry	[1] μM	[CAN] mM	[NaIO$_4$] mM	TOF$_I$ min^{-1}	TOF$_{LT}$ min^{-1}	TON
1	2.5	5	-	16	3	330
2	2.5	10	-	33	5	510
3	5.0	5	-	13	4	225
4	5.0	10	-	22	4	450
5	10.0	5	-	21	6	100
6	1	20	-	190	-	180
7	1	40	-	301	-	200
8	2.5	5	-	42	-	80
9	2.5	10	-	98	-	100
10	5	5	-	25	-	20
11	5	10	-	62	-	60
12	10	5	-	18	-	25
13	10	10	-	19	-	55
14	2.5	5	-	-	9	301
15	2.5	10	-	-	10	784
16	5	5	-	-	8	250
17	5	10	-	-	10	485
18	10	5	-	-	7	110
19	10	10	-	-	10	234
20	1	-	20	-	69	6340
21	2.5	-	20	-	85	3130
22	5	-	20	-	95	1925
23	10	-	20	-	89	925
24	5	-	5	-	38	500
25	5	-	10	-	67	1000
26	5	-	40	-	167	3366

UV-Vis kinetic trends revealed a discontinuity occurring after some minutes (SI, Figure S12) that allowed defining an initial (TOF$_I$) and long-term (TOF$_{LT}$) turnover frequency,

when CAN was used as sacrificial oxidant. This is likely due to the oxidative transformation of the catalytic active species during catalysis.[20,42,43,44,45,46,47,48] TOF_I was better evaluated by Clark electrode (SI, Figure S10) because of its sensitive to initial small variations in the dissolved oxygen concentration but the method becomes poorly quantitative at higher extent of reaction due to the formation of undetectable oxygen bubbles. Therefore, TOF_{LT} was also evaluated with manometry. TOF_I was found to roughly doubles when the concentration of CAN was doubled (compare entries 1-2, 3-4, 8-9, and 10-11 in Table 1) indicating a first-order dependence of WO in CAN. The order in **1** cannot be determined with certainty because an increase of concentration of **1** causes an apparent decrease of TOF_I determined with Clark electrode (compare entries 8, 10 and 12 or 9, 11 and 13, in Table 1), reasonably due to a higher production of O_2 bubbles at higher catalyst concentration. Nevertheless, TOF_I determined with UV-Vis remains roughly constant when **1** concentration increases (compare entries 1, 3 and 5 or 2 and 4 in Table 1), pointing toward an order equal to 1. Some catalytic experiments were carried out with Clark electrode, under conditions to maximize performances and detectability. In particular, when [CAN] was equal to 20 mM and 40 mM and [**1**] = 1 μM (entries 6 and 7 in Table 1), TOF_I reached 190 min^{-1} and 301 min^{-1}, respectively. Interestingly, the initial activity of **1** is almost twice higher than that of **2** (Figure 1A), which is the fastest iridium catalyst for WO driven by CAN, to the best of our knowledge.[22] TOF_{LT} determined by both UV-Vis and manometry exhibits a zero order with respect to CAN and first order with respect to **1** (entries 1-5 and entries 14-19 in Table 1; SI, Figure S12). For instance, the trends of TON *versus* t for two different experiments, in which the concentration of [**1**] was 5 μM and [CAN] was 5 mM and 10 mM (Entries 16 and 17, Table 1 and SI, Figure S11), showed almost the same slope with an average TOF_{LT} = 9 min^{-1}.
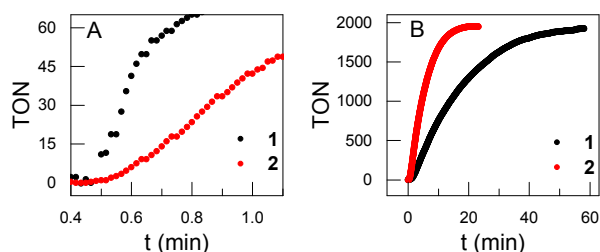

Figure 1. Comparison of activity between **1** and **2** catalysts in WO driven by CAN (A, [CAN] = 20 mM, [Cat] = 1 μM, pH 1 by HNO₃) and NaIO₄ (B, [NaIO₄] = 20 mM, [Cat] = 5 μM, pH 7 by phosphate buffer).

WO experiments driven by NaIO₄ revealed a first-order dependence in **1** (entries 20-23 in Table 1) and a fractional order in NaIO₄ (entries 22 and 24-26 in Table 1; SI, Figure S13), close to 0.7, as observed for **2** and its derivatives having the OH-substituents in different positions of the pyridine ring. The activity of **1** is remarkable not only because of the

high TOF (up to 167 min^{-1}, about half of that of the fast catalyst reported so far,[36] Figure 1B) but also because all expected cycles, based on the concentration of NaIO₄, were accomplished.

Hydrogenation of NAD⁺. NADH and NADPH are widely used as cofactors in many chemical and pharmaceutical biocatalytic processes.[49] Particularly, they act as hydride sources in bioreduction processes and, due to their high cost, it would be highly desirable to regenerate them. This can be accomplished through several methods including the exploitation of organometallic complexes as catalysts and molecular hydrogen as the hydride source.[50]

Complex **1** was tested as catalyst toward β-NAD⁺ (Scheme 2) hydrogenation, using HCOOK as hydride source (eq. 2).

$$\beta\text{-NAD}^+ + \text{HCOOK} \rightarrow 1,4\text{-}\beta\text{-NADH} + CO_2 + K^+ \qquad (2)$$
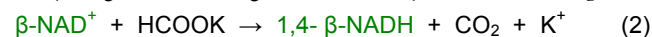
The reaction was monitored following the formation of β-NADH, by means of UV-Vis spectroscopy, and both the depletion of β-NAD⁺ and production of β-NADH by NMR. Results are reported in Table 2.
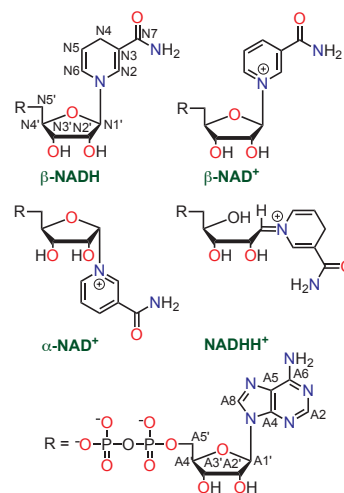
Scheme 2. NAD and NAD⁺ structures and labeling.

The reaction, which did not occur at all in the absence of **1**, led to the regiospecific formation of 1,4-NADH as demonstrated by ¹H NMR studies, which showed the formation of a single set of resonances with the diagnostic one at 2.6 ppm assigned to the diastereotopic N4-protons (Figure 2).
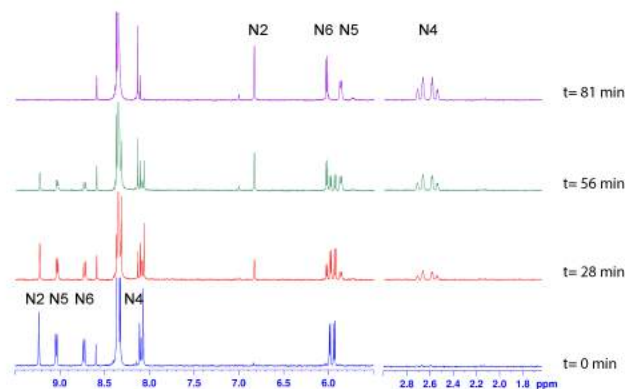
Figure 2. ^{1}H NMR spectra for the hydrogenation of NAD^{+} with HCOOK at different reaction times, catalyzed by **1**, showing the regioselective formation of 1,4-NADH ([NAD^{+}] = 2 mM, [**1**] = 26.2 μM, [HCOOK] = 125 mM, pH 7 by phosphate buffer).

The effect of pH in the catalytic activity of **1** toward reaction 2 was investigated in the 3.3 – 8 range (Table 2, entries 1-4, Figure 3A; SI, Figure S14). A maximum of activity was observed at pH 7 (TOF = 143 h^{-1}). At this pH, TOF was found to markedly decrease by an increase of the concentration of NAD^{+} (Table 2, entries 5-9), which is in strict analogy to what was found by Fukuzumi who attributed such an effect to the coordination of NAD^{+} at the catalyst.[34] The binding constant (K_M) was derived (K_M = 4.03 x 10^{3} M^{-1}) by plotting 1/TOF as a function of the concentration of NAD^{+} (Figure 3B), according to the literature procedure.[34]
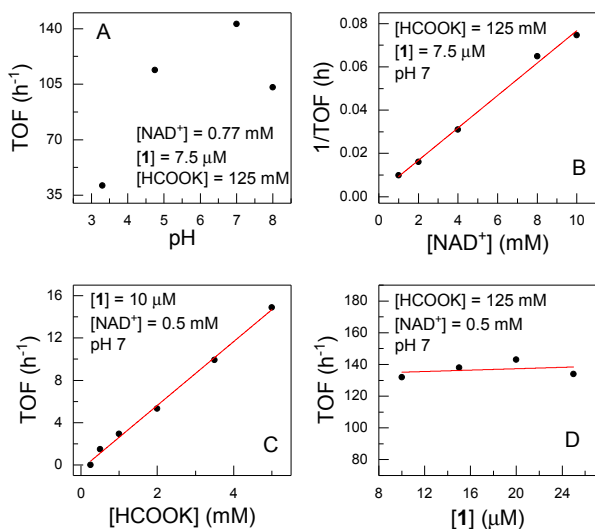

**Figure 3**. Effects of pH and NAD^{+}, HCOOK and **1** concentrations on reaction 2.

Table 2. Kinetic data for the hydrogenation of NAD^{+} with HCOOK catalyzed by 1 (25 °C, H₂O, phosphate buffer).

Entry	pH	[**1**] (μM)	[NAD^{+}] (mM)	[HCOOK] (mM)	TOF (h[-1])
1	3.3[a]	7.5	0.77	125	41
2	4.75[a]	7.5	0.77	125	114
3	7	7.5	0.77	125	143
4	8	7.5	0.77	125	103
5	7	10	1	125	102
6	7	10	2	125	62
7	7	10	4	125	32
8	7	10	8	125	15
9	7	10	10	125	13
10	7	10	0.5	0.25	0.7
11	7	10	0.5	0.5	1.4
12	7	10	0.5	1	2.9
13	7	10	0.5	2	5.3
14	7	10	0.5	3.5	9.9
15	7	10	0.5	5	14.9
16	7	10	1	125	132
17	7	15	1	125	134
18	7	20	1	125	143
19	7	25	1	125	134

[a]Measurement performed in phthalate buffer.

Kinetic orders in both HCOOK (Table 2, entries 10-15, Figure 3C; SI, Figure S15) and **1** (Table 2, entries 16-19, Figure 3D) were found to be 1 (SI, Figure S16). Based on the kinetic results and literature data by Sadler[29] and Fish,[51] the following catalytic cycle can be proposed for the reduction of NAD^{+} through transfer hydrogenation with HCOOK (Scheme 3).
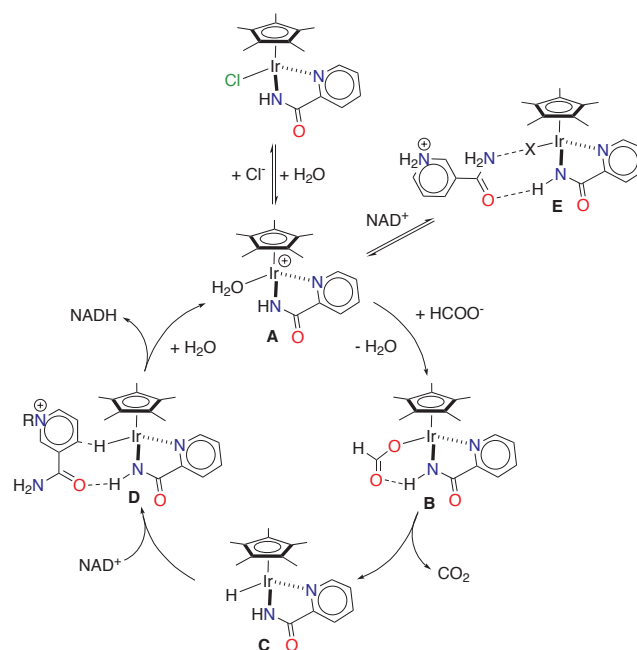
Scheme 3. Proposed mechanism for the hydrogenation of NAD^{+} with HCOOK catalyzed by 1.

Initially, water substitutes Cl^{-} leading to complex **A**, which reacts with HCOO[–] forming **B** or undergoes reversible coordination of NAD^{+}, affording the adduct **E**, an out-of-cycle species, which slows down the reaction when the concentration of NAD^{+} increases (X might be a water molecule or even coordination vacancy). Direct evidence for the formation of the adduct **E** was obtained by the detection of dipolar contacts between N2 and N6 protons of NAD^{+} and Cp* and H6 protons of the iridium moiety in the ^{1}H NOESY NMR (Figure 4). The presence of NOE contacts between the catalyst and two rather distant protons of NAD^{+}, N2 and N6, suggests that the latter can approach the catalyst in two different orientations as shown in Figure 4. The formation of **B** is likely favored by a hydrogen bond interaction between the oxygen atom of the carboxylic moiety and coordinated –NH. β-

elimination of hydrogen from **B**, accompanied by CO_2 evolution, leads to the hydric species **C** (**1_H**) that quickly hydrogenates NAD$^+$, liberating NADH and regenerating the aquo-complex **A**. Reacting **1** with HCOOK in water confirmed the formation of **1_H** (SI). After a few minutes a hydride resonance appeared at -11.5 ppm related at all set of resonances expected for **1_H** (SI, Figures S7 and S8). The observed value for the hydride resonance is in excellent agreement with that reported by Do and co-workers for an analogous iridium-pyridincarboxamidato complex.[35]

It is reasonable to believe that hydrogen bonding between the carbonyl of NAD$^+$ and –NH plays a role in facilitating NAD$^+$ coordination and hydrogenation in **D**. Consistently, at acidic pH, where –NH is reasonably protonated, a lower activity of **1** was observed. The decrease of activity at basic pH might be also due to the deprotonation of coordinated water in **A** leading to an Ir–OH complex which makes the coordination of COO$^-$ more difficult.
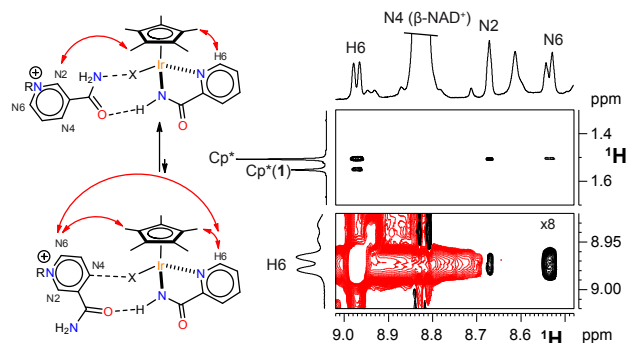

Figure 4. Two sections of the ^{1}H NOESY NMR spectrum (D$_2$O, pH 4.2 by phthalate, 25°C) showing the contacts between α-NAD$^+$ and the iridium protons in **E**.

In order to verify if the presence of the NH-functionality is indeed beneficial to the catalytic performances, a catalytic experiment was carried out under the conditions at which **1** exhibited the maximum TOF ([Catalyst] = 7.5 μM, [HCOOK] = 0.125 M, [NAD$^+$] = 0.77 mM, pH = 7, T = 25°C) using **2** instead of **1** as catalyst. The observed TOF value was 17 h^{-1}, almost one order of magnitude lower than that **1**, suggesting that the NH-functionality plays a key role in the hydrogenation process (SI, Figure S17).

In terms of performance, the best catalysts for reaction 2 are those based on rhodium that reached TOF as high as 2000 h^{-1} ([Cp*Rh(phen)Cl], phen = 1,10-phenantroline, at 60 °C),[27] whereas ruthenium catalysts exhibit TOF = 0.0056–10 h^{-1} at 37 °C.[29] As far as iridium is concerned, the fastest catalyst has been reported by Fukuzumi ([Cp*Ir(4-(1H-pyrazol-1-yl-κN^2)benzoic acid)(H$_2$O)]SO$_4$, **3**, Chart 1) that shows a TOF = 54 h^{-1} at room temperature and pH 7.[34] Under exactly the same conditions, catalyst **1** exhibits a TOF = 143 h^{-1}, which is about three times higher than that of **3**. This seems to be due to the higher tendency of **3** to form the out-of-cycle

species **E**.[34] As a matter of fact, K$_M$ for **3** (1.4x10^4 M^{-1}) is almost three times larger than that for **1** (4.04x10^3 M^{-1}).

Dehydrogenation of NADH. The dehydrogenation of β-NADH (eq. 3) catalyzed by **1**, under slightly acidic conditions, was investigated by NMR spectroscopy following the depletion of β-NADH and formation of nicotinamide species and by GC, monitoring the formation of H$_2$.

$$\beta\text{-NADH} + H^+ \rightarrow \beta\text{-NAD}^+ + H_2 \qquad (3)$$
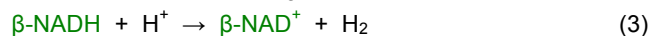
a) NMR kinetic and structural investigation. NMR studies indicate that the reaction is by far more complex than that depicted in eq. 3 and many nicotinamide species form, as illustrated in Scheme 4. Beside the expected oxidation product, β-NAD$^+$, immediately identifiable by the diagnostic singlet at 9.25 ppm (Figure 5A), another species missing the CH$_2$ moiety of the pyridine ring, having an analogous singlet at 8.98 ppm, was observed. An in-depth NMR study, paralleled with a strict comparison with authentic sample, allowed to unequivocally assigning such a species to α-NAD$^+$ (SI, Figure S18). The formation of α-NAD$^+$ is known to occur through the acid catalyzed anomerization of β-NADH to α-NADH, involving the acyclic iminium NADHH$^+$ intermediate (Scheme 4), followed by the dehydrogenation of α-NADH to α-NAD$^+$.[52]

Other un-oxidized, and NADH-like, species, featuring a broad signal at δ = 2.48 ppm, were observed and assigned to the product of hydration of NADH pyridine ring (NADHX in Scheme 4),[53,54,55] by comparison of our NMR data with ^{1}H [54] and ^{13}C [56] data reported in the literature.
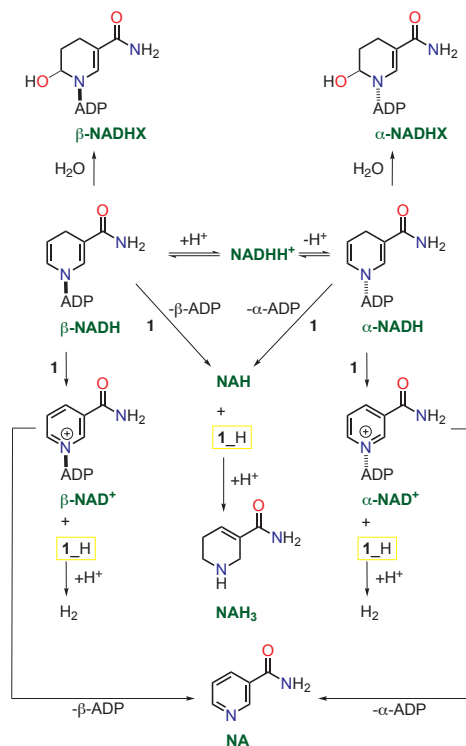
Scheme 4. Speciation of β-NADH during the dehydrogenation reaction, as deduced by NMR experiments.

Two additional species were observed. The first one exhibited proton and carbon resonances typical of the C-H aromatic moieties of a pyridine ring. The latter did not show any dipolar or scalar correlation with low-frequency aliphatic resonances. Furthermore, diffusion NMR experiments[57,58,59,60] pointed toward a much smaller hydrodynamic volume (V_H = 246 Å^3) than that expected and measured (1200-1300 Å^3) for a NAD$^+$-species (Figure 5B). Those findings and comparison with an authentic sample unequivocally indicate the formation of nicotinamide (NA in Scheme 4). The formation of NA is reasonable since the cleavage of the nicotinamide-ribosyl bond of NAD$^+$ is well documented in the literature, even if it usually occurs in the presence of a suitable enzyme or under basic conditions.[61,62,63,64]
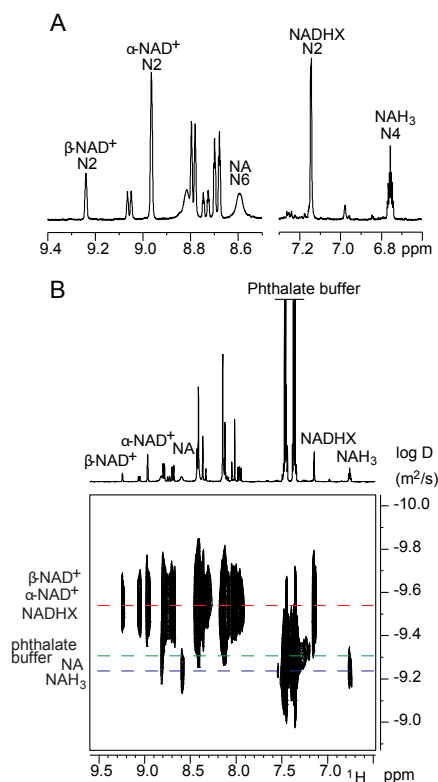

Figure 5. A: Two sections of the ^{1}H NMR spectrum (D$_2$O, pH 4.2 by phthalate, 25°C) of the dehydrogenation of β-NADH, showing the diagnostic resonances of each species allowing their quantification. B: A section of the ^{1}H-DOSY NMR (D$_2$O, pH 4.2 by phthalate buffer, 25°C) spectrum showing the difference in self-diffusion translation coefficient of NAD-species and NA and NAH$_3$.

The assignment of the second additional species was somewhat more problematic. By combining all pieces of information coming from ^{1}H and ^{13}C 1D- and 2D-NMR experiments, it was deduced that such a species has three CH$_2$-moieties, a CH-moiety and, consequently, only a double bond in the pyridine ring. Furthermore, because two CH$_2$-carbon resonances fall at rather similar and high frequency values (39.9 ppm and 40.8 ppm) (Figure 6C, ^{13}C JMOD vertical projection), consistent with carbons in N2 and N6 posi-

tions, it appears that a double bond has to be established between N3 and N4 carbons. The definitive assignment of such species came, again, from diffusion NMR experiments that indicated, also in this case, a V_H = 268 Å^3 (Figure 5B), only marginally higher than that of NA, consistent with the loss of the ADP-ribose fragment. In summary, this second additional species is 1,2,5,6-tetrahydronicotinamide (NAH$_3$) (Scheme 4).

The formation of NAH$_3$ is rather intriguing for several reasons. First, it is well-known that the hydrogenation of NADH to the tetrahydro derivative is an extremely difficult process asking for rather harsh conditions.[65,66,67] Second, NAH$_3$ has been rarely obtained using transition metal hydrides as mediators.[68,69] Finally, most of the reports, with a few exceptions,[70] suggest the formation of 1,4,5,6-tetrahydronicotinamide derivatives, whereas 1,2,5,6-tetrahydronicotinamide forms, according to our NMR studies. Interestingly, Miller and co-workers recently showed that MNAH$_3$ (1-methyl-1,4,5,6-tetrahydronicotinamide) can be generated via the photo hydride transfer from [Cp*Ir(bpy)H]OTf to MNA.[69]

β-NAD$^+$, α-NAD$^+$, NADHX, NA and NAH$_3$ account for 90-95 % of initial β-NADH with relative abundances, at the end of the reaction, which clearly depend on the experimental conditions but in all cases α-NAD$^+$ prevalently forms paralleled by NAH$_3$, when catalyst concentration is low, as discussed below.

In order to understand if this capability of causing such a broad speciation of β-NADH is a peculiarity of **1**, analogous NMR experiments were repeated using **3**, which is one of the best iridium catalysts for β-NADH dehydrogenation reported so far.[34] Substantially, the same speciation was observed (SI, Figure S19).
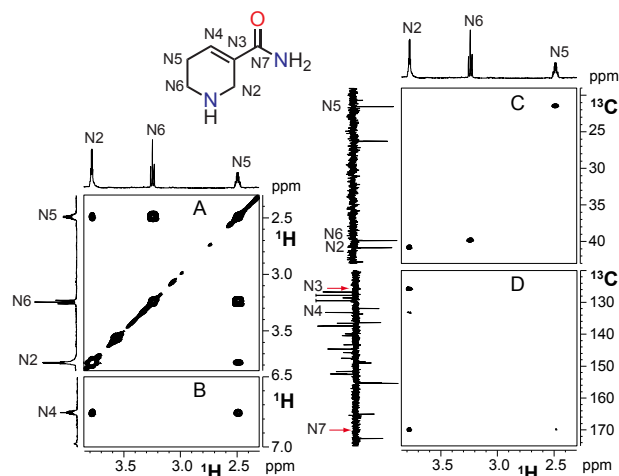

Figure 6. Sections of the ^{1}H,^{1}H-COSY (A and B), ^{1}H,^{13}C-HSQC (C) and ^{1}H,^{13}C-HMBC (D) NMR spectra (D$_2$O, pH 4.2 by phthalate buffer, 25°C) showing the scalar connectivity in NAH$_3$.

Although the resulting picture is extremely complex, NMR kinetic studies were performed following the formation of β-

NAD$^+$, α-NAD$^+$, NAH$_3$ and ADP. Data are reported in Table 3. Due to the presence of many species and the consequent overlapping of resonances, integration was in some cases affected by a higher degree of uncertainty than usual. This was also reflected in the accuracy of kinetic data but this did not compromise the possibility of obtaining mechanistic information.

As far as the direct oxidation of β-NADH to β-NAD$^+$ is concerned, it was found to be roughly first order with respect to NADH (Table 3, entries 1 and 5-7) and **1** (Table 3, entries 8-13) and little dependent on the H$^+$ (Table 3, entries 1-4; SI, Figure S20, apparent order 0.2).

The Kinetic Isotopic Effect (KIE) was evaluated by performing reaction 3 in H$_2$O, under exactly the same conditions as in D$_2$O (pH 4.2, [NADH] = 10 mM, [**1**] = 0.2 mM; Table 3, entries 11 and 12). k_{obs}^β passed from 44 μM/min to 114 μM/min with a KIE = 2.6 (SI, Figure S21). This, together with the determined kinetic law, which indicates a first order in both **1** and NADH, points to the interaction of NADH with the catalyst, leading to the hydride species **1**-H, as the, likely reversible, rate determining step (rds).

Table 3. NMR determined k_{obs} (μM/min) for the dehydrogenation of β-NADH (mM) catalyzed by 1 (mM) (25 °C, D$_2$O, phthalate buffer).

	pH	[**1**]	[NADH]	k_{obs}^α	k_{obs}^β	k_{obs}^{NAH3}	k_{obs}^{ADP}
1	4.2	0.2	10	133	44	76	40
2	5	0.2	10	29	26	19	10
3	6[a]	0.2	10	7	12	4	3
4	7[a]	0.2	10	1	5	1	1
5	4.2	0.2	2	30	13	18	7
6	4.2	0.2	4	34	24	27	10
7	4.2	0.2	8	72	35	50	22
8	4.2	0.04	10	63	3	11	9
9	4.2	0.1	10	168	17	52	25
10	4.2	0.2	10	133	44	76	40
11[b]	4.2	0.2	10	165	114	-	-
12	4.2	0.4	10	91	53	69	32
13	4.2	1.34	10	142	107	132	50

[a]Measurement performed with phosphate buffer. [b]Measurement performed in H$_2$O.

The formation of α-NAD$^+$ was found to be first order with respect to NADH (Table 3, entries 1 and 5-7) and H$^+$ (Table 3, entries 1-4) but zero order with respect to **1** (Table 3, entries 8-13; SI, Figure S22). Furthermore, KIE was only marginally higher than 1 (SI, Figure S23). All experimental findings consistently indicate that the acid-catalyzed anomerization of β-NADH to α-NADH is the rate determining step of α-NAD$^+$ formation. Involvement of **1** in the rds can be ruled out by its zero order and KIE ≈ 1.

Also the formation of NAH$_3$ (SI, Figure S24) and ADP (SI, Figure S25) was found to be first order in both NADH (Table 3, entries 1 and 5-7) and catalyst (Table 3, entries 8-13).

According to the above-reported kinetic results, the reaction mechanism reported in the central section of Scheme 4 can be proposed. It points out that β-NADH may undergo three competitive reactions: i) donation of a hydride to **1** forming β-NAD$^+$ and **1_H**; ii) acid catalyzed anomerization to α-NADH, followed by the interaction of α-NADH with **1**, leading to α-NAD$^+$ and **1_H**; iii) **1** catalyzed cleavage of the nicotinamide-ribosyl bond. In both i) and ii) pathways, **1_H** reacts with H$^+$ generating H$_2$ and it is worth noticing that reaction ii) always occurs faster than reaction i), under the studied experimental condition (pH 4.2), and has in the acid catalyzed anomerization of β-NADH to α-NADH its slowest step. This indicates that dehydrogenation is considerably faster in α-NADH than in β-NADH. Such a difference is further accentuated at low concentration of catalyst, because only the dehydrogenation of β-NADH exhibits a first-order dependence on **1**. For instance, $k_{obs}^\alpha/k_{obs}^\beta$ = 21 when [**1**] = 0.04 mM and [NADH] = 10 mM (Table 3, entry 8).

The formation of **1_H** though the hydride transfer from β-NADH was ascertained by reacting **1** with 5 equivalents of β-NADH in basic conditions (SI). The diagnostic resonance at -11.5 ppm was visible after having warmed up the water solution (SI, Figure S9).

As far as the formation of NAH$_3$ is concerned, three pathways might be considered: 1) the hydrogenation of NADH to NADH$_3$ followed by the cleavage of the nicotinamide-ribosyl bond, 2) the cleavage of the nicotinamide-ribosyl of NADH, leading to NAH, followed by the hydrogenation of the latter to NAH$_3$, and 3) the hydrogenation of NA. Several attempts to hydrogenate NA with **1**, in the presence of H$_2$ at atmospheric pressure, or adding NADH were performed but they were all unsuccessful. This makes pathway 3) improbable. The discrimination between pathway 1) and 2) is not simple. However, the observed first order in NADH and catalyst for both NAH$_3$ and ADP formation is consistent with pathway 2) being more probable (Scheme 4).

b) GC kinetic investigation. The kinetics of H$_2$ evolution was studied by means of GC under conditions directly comparable with those used in NMR experiments (Table 4, entries 1-6) but also under conditions identical to those used by Fukuzumi[34] (Table 4, entries 7-12). It appears that TOF slightly decreases as the concentration of **1** is increased (Table 4, entries 1-4 and 7-9) suggesting a fractional order in catalyst (determined to be 0.47 and 0.77 from $\log k_{obs}/\log[\textbf{1}]$ plots in the two NADH concentration regimes; SI, Figures S26 and S28). This is consistent with the NMR observation of 1 and 0 order for **1** in the production β-NAD$^+$ and α-NAD$^+$, respectively, because both processes produce H$_2$.

Changing the NADH concentration does not significantly affect the TOF of H$_2$ evolution at [**1**] = 0.200 mM (Table 4,

entries 4-6), suggesting zero order in NADH (SI, Figures S27 and S29). Whereas, at [**1**] = 0.065 mM an increase of NADH concentration is detrimental, indicating a negative order in NADH. This appears difficult to explain but could be related to the formation of NAH_3 as discussed below.

The amount of evolved H_2 is considerably smaller than that expected based on NAD^+ formation (SI, Figures S30), because part of it is consumed to produce NAH_3. It was mentioned before that, at low concentration of **1**, k_{obs}^{α} is much higher than k_{obs}^{β} and, at the same time, the final amounts of H_2 and NAH_3 are similar to those of α-NAD^+ and β-NAD^+, respectively. For instance, at [NADH] = 3.3 mM and [**1**] = 0.015 mM the TON for the formation of α-NAD^+ is 25, consistent with that of H_2 (23, entry 7 in Table 4). At the same time, an identical TON = 7 was observed for β-NAD^+ and NAH_3 formation. This is reasonable because when the catalyst amount is small, α-NADH forms, but it does not accumulate, readily producing **1**_H. The latter has the possibility to interact with H^+, producing H_2, or to hydrogenate NAH leading to NAH_3.

Table 4. GC kinetic data for the evolution of H_2 catalyzed by 1 (25 °C, H_2O, pH 4.2 by phthalate buffer).

Entry	[**1**] (mM)	[NADH] (mM)	TOF (min⁻¹)	TON
1	0.025	10	0.38	10
2	0.050	10	0.31	6
3	0.100	10	0.18	4
4	0.200	10	0.14	2
5	0.200	5	0.18	2
6	0.200	2.5	0.17	2
7	0.015	3.3	0.33	23
8	0.034	3.3	0.30	11
9	0.065	3.3	0.24	6
10	0.065	1	0.29	5
11	0.065	5	0.23	6
12	0.065	10	0.16	5

Some catalytic experiments were carried out to compare the performance of **1** with that of **3**, which is the best iridium catalyst for the dehydrogenation of NADH reported so far,[34] under exactly the same experimental conditions. At [cat] = 0.2 mM and [NADH] = 10 mM, the two catalysts exhibit similar TOF values (0.14 min⁻¹ for **1** and 0.16 min⁻¹ for **3**) although **3** (TON = 3.5) produces more H_2 than **1** (TON = 2). **3** (TOF = 0.63 min⁻¹; TON = 7) exhibits better performances than **1** (TOF = 0.2 min⁻¹; TON = 6), by lowering the concentrations down to [cat] = 0.065 mM and [NADH] = 3.3 mM, especially in terms of TOF whereas TON are comparable (Figure 7).
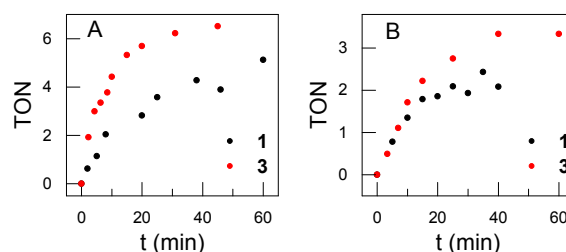

Figure 7. Comparison of performances for catalysts **1** and **3** under exactly the same experimental conditions.

CONCLUSIONS

The results herein reported demonstrate that a single organometallic complex, namely [Cp*Ir(pica)Cl] (**1**), is able to efficiently catalyze all processes that are keys to light-dependent, electron transfer reactions of Z scheme of oxygenic photosynthetic organisms. This means that **1** is a functional mimic of both OEC (Oxygen Evolving Complex) and ferredoxin/ferredoxin NAD^+ reductase. Catalytic performances in water oxidation driven by CAN and $NaIO_4$ and NAD^+ hydrogenation are among the highest reported for an iridium complex. Particularly, the success in the latter reaction seems to be strictly related to the presence of the NH-functionality that allows the establishment of beneficial intermolecular hydrogen bonding between the $HCOO^-$ and the catalyst.

The complex **1** efficiently catalyzes the dehydrogenation of β-NADH, too, leading to H_2 evolution with performances that well compare with those of the best catalysts. Importantly, NMR kinetic and structural analysis revealed an unexpected complexity of such a reaction leading to many species, which were all assigned. Such a complexity appears to be rather general, as indicated by the fact that it was also observed when **3** was used as the catalyst. The final kinetic picture suggests that most of H_2 is produced passing through the acid catalyzed anomerization of β-NADH to α-NADH followed by the dehydrogenation of the latter. Both α-NADH and β-NADH donates the hydride to **1**, forming **1**_H, but this process was found to occur much faster for the former. Beside the productive reaction of **1**_H with H^+, a competitive reaction was observed involving the hydrogenation of NAH by **1**_H and H^+. The latter leads to the formation of NAH_3, which limits the yield of H_2.

ASSOCIATED CONTENT

Supporting Information

AUTHOR INFORMATION

Corresponding Author

*E-mail: alceo.macchioni@unipg.it. Web: http://www.unipg.it/ pagina-personale?n=alceo.macchioni.

Present Addresses

†Institute of Chemical Research of Catalonia (ICIQ), The Barcelona Institute of Science and Technology, Avinguda Països Catalans 16, 43007 Tarragona, Spain.

§Dartmouth College, Department of Molecular and Systems Biology, Program in Experimental and Molecular Medicine, 7400 Remsen, Hanover, NH 03755, USA.

REFERENCES

(1) Armaroli, N.; Balzani, V. *Chem. Eur. J.* **2016**, *22*, 32-57 and references therein.

(2) Su, J.; Vayssieres, L. *ACS Energy Lett.* **2016**, *1*, 121-135 and references therein.

(3) Brennaman, M. K.; Dillon, R. J.; Alibabaei, L.; Gish, M. K.; Dares, C. J.; Ashford, D. L.; House, R. L.; Meyer, G. J.; Papanikolas, J. M.; Meyer, T. J. *J. Am. Chem. Soc.* **2016**, *138*, 13085-13102 and references therein.

(4) Rongé, J.; Bosserez, T.; Martel, D.; Nervi, C.; Boarino, L.; Taulelle, F.; Decher, G.; Bordiga, S.; Martens, J. A. *Chem.Soc.Rev.* **2014**, *43*, 7963-7981.

(5) Barber, J.; D. Tran, P. D. *J. R. Soc. Interface* **2013**, *10*, 20120984/1-20120984/16.

(6) *Molecular Mechanisms of Photosynthesis*, Blankenship, R. E.; Blackwell Science: Oxford, (UK), 2002.

(7) Barber, J. *Biochemistry* **2016**, *55*, 5901-5906 and references therein.

(8) Askerka, M.; Brudvig, G. W.; Batista, V. S. *Acc. Chem. Res.* **2017**, 10.1021/acs.accounts.6b00405 and references therein.

(9) Karplus, P. A.; Daniels, M. J.; Herriott, J. R. *Science* **1991**, *251*, 60-6.

(10) Wang, M.; Roberts, D. L.; Paschke, R.; Shea, T. M.; Masters, B. S. S.; Kim, J.-J. P. *Proc. Natl. Acad. Sci. USA* **1997**, *94*, 8411-8416.

(11) Koo, J.; Schnabel, T.; Liong, S.; Evitt, N. H.; Swartz, J. R. *Angew. Chem., Int. Ed.* **2017** DOI:10.1002/anie.201610260 and references therein.

(12) Nocera, D. G. The Artificial Leaf *Acc. Chem. Res.* **2012**, *45*, 767-776.

(13) Hull, J. F.; Balcells, D.; Blakemore, J. D.; Incarvito, C. D.; Eisenstein, O.; Brudvig, G. W.; Crabtree, R. H. *J. Am. Chem. Soc.* **2009**, 131, 8730-8731.

(14) Blakemore, J. D.; Schley, N. D.; Balcells, D.; Hull, J. F.; Olack, G. W.; Incarvito, C. D.; Eisenstein, O.; Brudvig, G. W.; Crabtree, R. H. *J. Am. Chem. Soc.* **2010**, 132, 16017-16029.

(15) Savini, A.; Bellachioma, G.; Ciancaleoni, G.; Zuccaccia, C.; Zuccaccia, D.; Macchioni, A. *Chem. Commun.* **2010**, 46, 9218-9219.

(16) Lalrempuia, R.; McDaniel, N. D.; Muller-Bunz, H.; Bernhard, S.; Albrecht, M. *Angew. Chem., Int. Ed.* **2010**, 49, 9765-8.

(17) Dzik, W. I.; Calvo, S. E.; Reek, J. N. H.; Lutz, M.; Ciriano, M. A.; Tejel, C.; Hetterscheid, D. G. H.; de Bruin, B. *Organometallics* **2011**, 30, 372-374.

(18) Hetterscheid, D. G. H.; Reek, J. N. H. *Chem. Commun.* **2011**, *47*, 2712-2714.

(19) Marquet, N.; Gaertner, F.; Losse, S.; Pohl, M. -M.; Junge, H.; Beller, M. *ChemSusChem* **2011**, *4*, 1598-1600.

(20) Savini, A.; Belanzoni, P.; Bellachioma, G.; Zuccaccia, C.; Zuccaccia, D.; Macchioni, A. *Green Chem.* **2011**, *13*, 3360-3374.

(21) Savini, A.; Bellachioma, G.; Bolaño, S.; Rocchigiani, L.; Zuccaccia, C.; Zuccaccia, D.; Macchioni, A. *Chem.Sus.Chem.* **2012**, *5*, 1415-1419.

(22) Bucci, A; Savini, A.; Rocchigiani, L.; Zuccaccia, C; Rizzato, S.; Albinati, A; Llobet, A.; Macchioni, A. *Organometallics* **2012**, *31*, 8071-8074.

(23) Steckhan, E.; Herrmann, S.; Ruppert, R.; Dietz, E.; Frede, M.; Spika, E. *Organometallics* **1991**, *10*, 1568-1577.

(24) Lo, H. C.; Leiva, C.; Buriez, O.; Kerr, J. B.; Olmstead, M. M.; Fish, R. H. *Inorg. Chem.* **2001**, *40*, 6705-6716.

(25) Hollmann, F.; Witholt, B.; Schmid, A. *J. Mol. Catal. B: Enzym.* **2003**, *19-20*, 167-176.

(26) Grau, M. M.; Poizat, M. P.; Arends, I. W. C. E.; Hollman, F. *Appl. Organomet. Chem.* **2010**, *24*, 380-385.

(27) Canivet, J.; Fink, G. –S.; Štěpnička, P. *Eur. J. Inorg. Chem.* **2007**, 4736-4742.

(28) Haquette, P.; Talbi, B.; Barilleau, L.; Madern, N.; Fosse, C.; Salmain, M. *Org. Biomol. Chem.* **2011**, *9*, 5720-5727.

(29) Soldevila, J. J.; Bruijnincx, P. C. A.; Habtemariam, A.; Clarkson, G. J.; Deeth, R. J.; Sadler, P. J. *Organometallics* **2012**, *31*, 5958-5967.

(30) Štěpnička, P.; Ludvìk, J.; Canivet, J.; Fink, G. –S. *Inorg. Chim. Acta* **2006**, *359*, 2369-2374.

(31) Govindaswamy, P.; Canivet, J.; Therrien, B.; Fink, G. –S.; Stepnicka, P.; Ludvìk, J. *J. Organomet. Chem.* **2007**, *692*, 3664-3675.

(32) Ganesan, V.; Sivanesan, D.; Yoon, S. *Inorg. Chem.* **2017**, DOI: 10.1021/acs.inorgchem.6b02474.

(33) Betanzos-Lara, S.; Liu, Z.; Habtemariam, A.; Pizarro, A. M.; Qamar, B.; Sadler, P. J. *Angew. Chem., Int. Ed.* **2012**, *124*, 3963-3966.

(34) Maenaka, Y.; Suenobu, T.; Fukuzumi, S. *J. Am. Chem. Soc.* **2012**, *134*, 367-374.

(35) A similar complex, [Cp*Ir(N-phenyl-2-pyridine-carboxamidate)Cl], has been recently exploited to mediate the hydrogenation of cytotoxic aldehydes by NADH: Ngo, A. H.; Ibañez, M.; Do, L. H. *ACS Catal.* **2016**, *6*, 2637-2641.

(36) Menendez Rodriguez, G.; Bucci, A.; Hutchinson, R.; Bellachioma, G.; Zuccaccia, C.; Giovagnoli, S.; Idriss, H.; Macchioni, A. *ACS Energy Lett.* **2017**, *2*, 105-110.

(37) González Miera, G.; Martínez-Castro, E.; Martín-Matute, B. *Organometallics* **2017**, DOI: 10.1021/acs.organomet.7b00220.

(38) Khusnutdinova, J. R.; Milstein, D. *Angew. Chem., Int. Ed.* **2015**, *54*, 12236−12273.

(39) Dubey, A.; Nencini, L.; Fayzullin, R. R.; Nervi, C.; Khusnutdinova, J. R. *ACS Catal.*, **2017**, *7*, 3864-3868.

(40) Zhao, B.; Han, Z.; Ding, K. *Angew. Chem., Int. Ed.* **2013**, *52*, 4744−4788.

(41) Watanabe, M.; Hori, J.; Murata, K. Patent EP 2228377 A1 20100915, November 3, 2010.

(42) Grotjahn, D. B.; Brown, D. B.; Martin, J. K.; Marelius, D. C.; Abadjian, M.-C.; Tran, H. N.; Kalyuzhny, G.; Vecchio, K. S.; Specht, Z. G.; Cortes-Llamas, S. A. *et al. J. Am. Chem. Soc.* **2011**, *133*, 19024-19027.

(43) Schley, N. D.; Blakemore, J. D.; Subbaiyan, N. K.; Incarvito, C. D.; D'Souza, F.; Crabtree, R. H.; Brudvig, G. W. *J. Am. Chem. Soc.* **2011**, *133*, 10473-10481.

(44) Zuccaccia, C.; Bellachioma, G.; Bolaño, S.; Rocchigiani, L.; Savini, A.; Macchioni, A. *Eur. J. Inorg. Chem.* **2012**, 1462-1468.

(45) Hintermair, U.; Sheehan, S. W.; Parent, A. R.; Ess, D. H.; Richens, D. T.; Vaccaro, P- H.; Brudvig, G. W.; Crabtree, R. H. *J. Am. Chem. Soc.* **2013**, *135*, 10837-10851.

(46) Ingram, A. J.; Wolk, A. B.; Flender, C.; Zhang, J.; Johnson, C. J.; Hintermair, U.; Crabtree, R. H.; Johnson, M. A.; Zare, R. N. *Inorg. Chem.* **2014**, *53*, 423-433.

(47) Zuccaccia, C.; Bellachioma, G.; Bortolini, O.; Bucci, A.; Savini, A.; Macchioni, A. *Chem.-Eur. J.* **2014**, *20*, 3446-3456.

(48) Corbucci, I.; Ellingwood, K.; Fagiolari, L.; Zuccaccia, C.; Elisei, F.; Gentili, P. L.; Macchioni, A. *Catal. Today* **2017**, *290*, 10–18.

(49) Wang, X.; Saba, T.; Yiu, H. H. P.; Howe, R. F.; Anderson, J. A.; Shi, J. *Chem* **2017**, *2*, 621–654.

(50) Quinto, T.; Köhler, V.; Ward, T. *Top. Catal.* **2014**, *57*, 321–331.

(51) Lo, H. C.; Leiva, C.; Buriez, O.; Kerr, J. B.; Olmstead, M. M.; Fish, R. H. *Inorg. Chem.* **2001**, *40*, 6705-6716.

(52) Oppenheimer, N. J. Everse, J.; Anderson, B.; You, K.-S., Eds.; Elsevier **1982**, 51-89.

(53) Johnson, S. L.; Tuazon, P. T. *Biochemistry* **1977**, *16*, 1175-1182.

(54) Oppenheimer, N. J.; Kaplan, N. O. *Biochemistry* **1974**, *13*, 4675-4685.

(55) Wu, J. T.; Wu, L. H.; Knight, J. A. *Clin. Chem.* **1986**, 32, 2, 314-319.

(56) Williams, T. J.; Ellis, P. D.; Bryson, T. A.; Fisher, R. R.; Dunlap, R. B. *Arch. Biochem. Biophys.* **1976**, *176*, 275-284.

(57) Ciancaleoni,G.; Zuccaccia, C.; Zuccaccia, D.; Macchioni, A. in Techniques in Inorganic Chemistry, ed. Fackler, Jr, J. P. ; Falvello, L. R. Boca Raton, 2010, pp. 129–180.

(58) Cohen, Y.; Avram, L.; Frish, L. *Angew. Chem., Int. Ed.* **2005**, *44*, 520.

(59) Macchioni, A.; Ciancaleoni, G.; Zuccaccia, C.; Zuccaccia, D. *Chem. Soc. Rev.* **2008**, *37*, 479.

(60) Avram, L. ; Cohen, Y. *Chem. Soc. Rev.* **2015**, *44*, 586.

(61) Oppenheimer, N. J. *Mol. Cell. Biochem.* **1994**, *138*, 245-251.

(62) Rising, K. A.; Schramm, V. L. *J. Am. Chem. Soc.* **1997**, *119*, 27- 37 and references therein.

(63) Liu, Q.; Kriksunov, I. A.; Jiang, H.; Graeff, R.; Lin, H.; Lee, H. C.; Hao, Q. *Chem. Biol.* **2008**, *15*, 1068–1078.

(64) Dudev, T.; Lim, C. J. Am. Chem. Soc. **2010**, *132*, 16533–16543.

(65) Yamada, S.; Kuramoto, M.; Kikugawa, Y. *Tetrahedron Lett.* **1969**, *10*, 3101-3104.

(66) Freifelder, M. *J. Org. Chem.* **1964**, *29*, 2895-2898.

(67) Rosentreter, U. *Synthesis* **1985**, 210-212.

(68) Okamoto, T.; Yamamoto, S.; Oka, S. *J. Mol. Catal.* **1987**, *39*, 219-223.

(69) Barrett, S. M.; Pitman, C. L.; Walden, A. G.; Miller, A. J. M. *J. Am. Chem. Soc.* **2014**, *136*, 14718–14721.

(70) Acheson, R. M.; Paglietti, G. *J. Chem. Soc., Perkin Trans. 1* **1976**, 45-48.

TOC